Influence of transport on two-dimensional model simulations: 2. Stratospheric aircraft perturbations

Eric L. Fleming,[1] Charles H. Jackman, David B. Considine,[2]

and Richard S. Stolarski
NASA Goddard Space Flight Center, Greenbelt, Maryland

Received _____; accepted _____

Submitted version: October 12, 1999

Short title: 2-D MODEL SIMULATIONS OF HSCT PERTURBATIONS

---

[1]Also at Steven Myers and Associates Corporation, Arlington, Virginia.

[2]Also at Department of Meteorology, University of Maryland, College Park.

Abstract.

We have adopted the transport scenarios used in Part 1 to examine the sensitivity of stratospheric aircraft perturbations to transport changes in our 2-D model. Changes to the strength of the residual circulation in the upper troposphere and stratosphere and changes to the lower stratospheric K_{zz} had similar effects in that increasing the transport rates decreased the overall stratospheric residence time and reduced the magnitude of the negative perturbation response in total ozone. Increasing the stratospheric K_{yy} increased the residence time and enhanced the global scale negative total ozone response. However, increasing K_{yy} along with self-consistent increases in the corresponding planetary wave drive, which leads to a stronger residual circulation, more than compensates for the K_{yy}-effect, and results in a significantly weaker perturbation response, relative to the base case, throughout the stratosphere. We found a relatively minor model perturbation response sensitivity to the magnitude of K_{yy} in the tropical stratosphere, and only a very small sensitivity to the magnitude of the horizontal mixing across the tropopause and to the strength of the mesospheric gravity wave drag and diffusion. These transport simulations also revealed a generally strong correlation between passive NO_y accumulation and age of air throughout the stratosphere, such that faster transport rates resulted in a younger mean age and a smaller NO_y mass accumulation. However, specific variations in K_{yy} and mesospheric gravity wave strength exhibited very little NO_y-age correlation in the lower stratosphere, similar to 3-D model simulations performed in the recent NASA "Models and Measurements" II ananlysis.

The base model transport, which gives the most favorable overall comparison with inert tracer observations, simulated a global/annual mean total ozone response of -0.59%, with only a slightly larger response in the northern compared to the southern hemisphere. For transport scenarios which gave tracer simulations within some agreement with measurements, the annual/globally averaged total ozone response ranged from -0.45% to -0.70%. Our previous 1995 model exhibited overly fast transport

rates, resulting in a global/annually averaged perturbation total ozone response of -0.25%, which is significantly weaker compared to the 1999 model. This illustrates how transport deficiencies can bias model simulations of stratospheric aircraft.

1. Introduction

Over the past decade, a variety of multi-dimensional chemistry and transport models (CTMs) have been used to study the impact of high speed civil transport (HSCT) aircraft emissions on stratospheric ozone [e.g., *Stolarski et al.*, 1995; *Kawa et al.*, 1999; *IPCC*, 1999]. Several factors are involved in proper model simulations of these HSCT effects. These include the quantification of nitrogen oxides, water, and aerosol particles emitted in the aircraft exhaust, and proper treatment of the atmospheric chemical processes influenced by these emissions.

An accurate representation of atmospheric dynamical processes is also vital for modeling supersonic aircraft effects. Variations in the transport of exhaust from the source regions in the mid-latitude lower stratosphere to other parts of the atmosphere can lead to significant variations in the amount of ozone destruction incurred. For example, exhaust transported to the troposphere will have little effect on ozone, whereas exhaust transported to the tropical stratosphere can ascend to higher altitudes and lead to greater ozone loss locally as well as globally. Proper determination of transport rates also has implications for modeling the long term accumulation of exhaust products throughout various regions of the stratosphere.

Because of the computational simplicity, two-dimensional (2-D) models have been widely used in assessments of these high altitude aircraft effects. The development and application of 2-D models to a variety of stratospheric problems have been previously documented [e.g., *Garcia and Solomon*, 1983; *Weisenstein et al.*, 1991; *Garcia et al.*, 1992; *Kinnison et al.*, 1994; *Stolarski et al.*, 1995; *Jackman et al.*, 1996; *Weisenstein et al.*, 1996; *Rosenfield et al.*, 1997; *WMO*, 1998; *Kawa et al.*, 1999; *IPCC*, 1999]. However, very few studies have specifically examined the role of dynamics in 2-D model simulations of stratospheric aircraft effects. *Jackman et al.* [1991] studied the dependence of varying the transport on 2-D model simulations of base total column ozone and the ozone perturbation due to HSCT NO_x injections, along with simulations

of inert radioactive tracers carbon-14 (^{14}C) and strontium-90 (^{90}Sr). Their simulations were strongly sensitive to the model dynamics such that weaker transport rates generally resulted in less ^{14}C removed from the stratosphere, and hence a longer emission residence time and greater ozone depletion.

In Part 1 of this study, we examined the impact of transport variations on long lived tracer simulations in our 2-D model. These included the dependence on the circulation and vertical diffusion in the upper troposphere and stratosphere, the horizontal diffusion in the middle atmosphere and around the tropopause, and the gravity wave-induced drag and vertical diffusion in the upper stratosphere and mesosphere. This study also allowed us to estimate a possible range of model transport rates that produce tracer simulations within reasonable agreement with observations.

In the present paper, we examine how these transport variations affect the model simulations of stratospheric aircraft perturbations. We will investigate the model simulated response in water vapor, NO_y, and ozone to changes in the transport fields. We will also examine the correlation between mean age and the perturbation responses in total ozone and inert NO_y accumulation for the different transport experiments. Based on the model-measurement comparisons of long lived tracers shown in Part 1, we can then determine a range of uncertainty due to transport in the model computed perturbation ozone response.

2. GSFC 2-D Model

The 2-D model at NASA/Goddard Space Flight Center (GSFC) was originally described in *Douglass et al.* [1989] and *Jackman et al.* [1990]. Recent improvements to the model have been discussed in *Jackman et al.* [1996], and upgrades to the transport are described in *Fleming et al.* [1999]. Details of the new transport formulation are contained in the Appendix in Part 1. We have also updated the model reaction rates and photolysis cross sections to the latest Jet Propulsion Laboratory (JPL) 1997

recommendations [*DeMore et al.*, 1997]. As described in Part 1 of this study, we have also made some minor modifications to our model hydrocarbon and HO_x chemistry.

3. Results

Throughout this section, we will show the perturbation response in H_2O, NO_y, and profile and total ozone from the different transport sensitivity tests described in Part 1. These scenarios are listed in Table 1, along with the hemispherically and globally averaged annual mean perturbation response in total ozone expressed in percentage change. For these simulations, the model has been run for 20 years to obtain a seasonally repeating steady state solution, with all results shown from the final year of the run. All runs are made for 2015 conditions of aircraft emissions and surface boundary conditions for the background atmosphere [*Kawa et al.*, 1999; *IPCC*, 1999]. These boundary conditions correspond to a total Cl_y loading of 3.0 ppbv and a total Br_y loading of 12.5 pptv. We will compare the reference simulation, which includes subsonic aircraft only, with the perturbation simulation which includes both supersonics and subsonics. For the simulations of supersonic aircraft, we assume a NO_x emission index (E.I.) of 5 g/kg, 500 airplanes, and a 10% gas-to-particle conversion of the SO_2 emission. These runs correspond to the NASA Atmospheric Effects of Supersonic Aviation (AESA) assessment scenarios 1 and 8, and the International Panel on Climate Change (IPCC) scenarios D and S1k.

Figure 1 shows the reference total ozone simulation (subsonics only) on the left-hand column, along with the perturbation total ozone response (supersonics+subsonics minus subsonics only) in the right-hand column. Here we show simulations from the baseline transport (middle panels) and the circulation sensitivity scenarios listed in Table 1 and discussed in Part 1. The reference total ozone of the base transport (scenario A) has been shown to compare reasonably well with TOMS data in simulating the overall seasonal and latitudinal variations [*Fleming et al.*, 1999]. The baseline perturbation

response is negative at all latitudes and seasons, maximizing in the polar regions of both hemispheres during spring and summer. The largest negative response (-3.4%) occurs in the southern polar region during October. The negative ozone response is due to a combination of enhanced NO_x and H_2O, with the latter inducing ozone loss because of increased HO_x radicals and increased occurrence of polar stratospheric clouds (PSCs). The hemispheric and annual mean perturbation response of this base scenario is slightly larger in the northern hemisphere (NH) (see Table 1), with a global mean response of -0.59%.

Simulations of the inert radioactive bomb product, carbon-14 (^{14}C), help illustrate how aircraft emissions are transported throughout our model stratosphere. ^{14}C has a source region similar to HSCT emissions, i.e., the lower stratosphere at NH middle and high latitudes. Comparisons of ^{14}C simulations with observations (shown in Part 1) are especially useful in diagnosing model accuracy in simulating HSCT effects. In Figure 2, we show the time evolution of our base transport ^{14}C simulation versus latitude at three stratospheric altitudes. The peak initial concentration near 23 km is slowly advected upwards in the tropics by the residual circulation, and appears at 31 km over the equator in July 1964 (9 months after initialization). Throughout the stratosphere, there is a general decay of ^{14}C with time due to the imposed tropospheric loss. At 17 km, a seasonal cycle is superimposed on this trend at mid-high latitudes of both hemispheres, with maximum mixing ratios occurring during late winter and spring. Since this level is below the peak in concentration, the maximum in the seasonal cycle is caused by downward advection of large mixing ratios from above. Following the passage of the initial pulse of maximum ^{14}C amounts early in the time period, the tropics appear to be isolated from higher latitudes at all levels. This is shown by the low tropical ^{14}C values characteristic of ascent of air from the troposphere.

The ^{14}C simulation in Figure 2 illustrates that material in the extratropical stratosphere in our model is primarily advected down from higher levels, with minimal

horizontal transport through the tropics. Therefore, the large negative response in total ozone in the southern hemisphere (SH) polar spring in Figure 1 (middle right panel) is primarily caused by the transport of HSCT emissions from the NH to the SH via the residual circulation, and not by horizontal mixing through the tropical stratosphere. This residual circulation mechanism advects the NO_x and H_2O emissions from the NH extratropical lower stratosphere upwards into the mesosphere, then horizontally to the SH, with the return descent into the lower stratosphere during winter.

Figure 3 shows vertical profiles of the annual mean perturbation response in water vapor, NO_y, and ozone at 45°N. Here we have plotted the responses in terms of percentage change (left column), and mixing ratio change (right column). The baseline transport scenario (solid line) shows the largest responses near 18 km, which is the altitude of peak HSCT emission. At this level, water vapor increases by almost 20% (0.8 ppmv), with a 17% (1.4 ppbv) increase in NO_y. The largest percentage change in ozone (-1.3%) occurs at 15-18 km, with the local maximum in concentration change (28 ppbv) occuring near 20 km.

The increase in H_2O diminishes with height and remains constant (0.25 ppmv) above about 35 km. The change in NO_y similarly decreases above the peak, but diminishes to zero above 50 km due to the imposed tropospheric loss. Note that the negative ozone response minimizes near 30 km, but again increases with height in the upper stratosphere due to the enhanced HO_x-ozone loss caused by the H_2O increases. There is also a small *decrease* in NO_y in the upper troposphere near 10 km. This results from the fact that the perturbed case (HSCTs+subsonics) assumes that there will be a roughly 11% decrease in subsonic air traffic in the troposphere [*IPCC*, 1999], and hence decreased NO_x emissions compared to the subsonics-only reference case.

As discussed in Part 1, simulations with the base line model transport give the best overall comparisons with tracer observations. In the following sections, we show how moderate and large changes away from this baseline transport affect the model

simulations of the aircraft perturbation response in NO_y, H_2O, and ozone. We will discuss how changes in the circulation, K_{yy}, and K_{zz} fields affect the simulations separately, and then in various combinations. We will also compare the results from our latest 1999 model with those obtained using the previous 1995 version of our model transport.

3.1. Sensitivity to the circulation

In this section examine the model sensitivity to changing the residual circulation throughout the troposphere and lower stratosphere (the K_{yy} and K_{zz} fields remain fixed). In these experiments, we have increased and then decreased the circulation strength away from the baseline by moderate and then large amounts in the region below 35 km. These are defined as scenarios B, C, D, and E as decribed in Table 1. As seen in Figure 1 (left-hand column), a stronger circulation leads to more total ozone at high latitudes, i.e., increased downwelling, with less ozone in the tropics, with the opposite result occuring with a weaker circulation. Also with a stronger (weaker) circulation, less (more) H_2O and NO_y from the HSCT emissions are contained in the lower stratosphere (Figure 3) so that the negative perturbation response in profile ozone and total column ozone (Figure 1, right-hand column) is weaker (stronger). This is also reflected in the hemispheric and global mean total ozone responses in Table 1. The global/annual average response ranges from -0.71% to -0.31% for the range of circulation strengths tested here. It is interesting that in the baseline (A) and strong circulation (D, E) cases, the NH and SH average perturbation responses are almost the same. However, the hemispheric average response becomes increasingly asymmetric (larger in the NH) with a weakening of the circulation. It appears that with weaker circulations, more of the emission remains confined to the NH source region, whereas increasingly stronger circulations re-distribute the emissions globally leading to similar responses in each hemisphere. [mention mean age changes here??]

As seen in Figure 3, the altitude of largest positive response in NO_y and H_2O remains at the altitude of the peak emission for all of the circulation sensitivity tests. Note that the very strong circulation gives the smallest ΔNO_y in absolute concentration, but gives the largest percentage change due to the decrease in the local background NO_y caused by the stronger circulation. The background concentrations of H_2O have significantly weaker gradients and are much less affected by transport changes, so that the absolute and percentage changes in H_2O have similar dependences on the transport rates.

3.2. Sensitivity to lower stratospheric K_{zz}

Observational studies [e.g., *Hall and Waugh*, 1997; *Mote et al.*, 1998], have estimated K_{zz} in the lower tropical stratosphere to be .01-.02 m^2/s, and we have adopted this value in our base model simulation (scenario A). In this section, we investigate the sensitivity to changing the K_{zz} values in the lower stratosphere away from this baseline value. The reference and perturbation total ozone simulations are shown in Figure 4 for minimum lower stratospheric K_{zz} values of 0.001, 0.1, and 1 m^2/s (scenarios F, G, and H), along with the base case. We found that using a minimum stratospheric K_{zz} smaller than 0.001 m^2/s does not change the model response in the diagnostic tracers and the HSCT perturbation so that this value appears to be the lower limit of K_{zz} in our model.

As seen in Figure 4, changing the minimum K_{zz} value by 3 orders of magnitude does not appreciably change the reference total ozone simulation. This is likely due to the fact that total column ozone is a vertically integrated quantity which is not strongly affected by changes in vertical diffusion. However, the total ozone perturbation varies dramatically between scenarios F and H. Similar to the circulation sensitivity, a larger K_{zz} removes more of the emission from the lower stratosphere, leading to a smaller negative total ozone response. For the smallest K_{zz} of 0.001 m^2/s, the NH, SH and global/annual mean responses are only slightly enhanced compared to the base case

(Table 1). For a moderately larger K_{zz} of 0.1 m^2/s, the negative responses are somewhat diminished at all latitudes. This is similarly seen in Figure 5 which shows that NO_y and H_2O undergo only small changes in scenarios F and G compared to the base case. However, increasing the minimum K_{zz} to 1 m^2/s (scenario H), dramatically reduces the perturbation response in NO_y and H_2O, and in total ozone throughout the globe (Figure 4). Scenario H also reveals that while ΔNO_y and ΔH_2O still exhibit maxima near 18 km, the change in ozone is negligible or even slightly positive in this region. This ozone increase likely results from the greatly reduced ΔH_2O, and hence, decreased HO_x loss of ozone, so that the increased NO_y leads to a slight net production of ozone in the lowest part of the stratosphere [*IPCC*, 1999]. However, we note that this scenario was concluded to be unrealistic as illustrated by comparisons with tracer observations in Part 1 [see also *Hall et al.*, 1999].

3.3. Sensitivity to mesospheric gravity wave effects

We examined the sensitivity of the HSCT simulations to varying the gravity wave drag and diffusion in the mesosphere. The model gravity wave parameterization (Appendix, Part 1) computes diffusion, used as the model K_{zz} field, and wave drag which has a direct effect on the model residual circulation. However, these processes were found to have the largest influence on tracers in the mesosphere, with very little effect on the lower and middle stratosphere (see Part 1). As listed in Table 1, sensitivity tests with weak and strong mesospheric gravity wave drag and diffusion (scenarios I and J) resulted in small changes, relative to the base case, in the hemispheric and global mean total ozone responses.

3.4. Sensitivity to stratospheric K_{yy}

Figure 6 shows the reference and perturbation responses in total ozone for different K_{yy} scenarios and the baseline model. Here we have decreased and increased the K_{yy}

values everywhere above the tropopause by constant factors of 2 and 5 (scenarios K, L, M, and N in Table 1). As expected, increasing K_{yy} generally reduces the latitudinal gradients in the reference total ozone plots. With a smaller K_{yy}, more of the emission remains confined near the NH source region. As a result, the total ozone perturbation response at NH high latitudes is largest with the smallest K_{yy}. South of about 50°N-60°N, the perturbation response increases with increasing K_{yy} as more of the emission is flushed out to the tropics and into the SH.

Since the HSCT emissions originate primarily at NH middle and high latitudes, changing K_{yy} does not strongly affect the NH average (Table 1). Conversely, the SH and global averages are enhanced dramatically with increasing K_{yy}. Interestingly, this increase in K_{yy} reaches a limit above which the response is not significantly effected, as seen by the fact that the K_{yy}*2 and K_{yy}*5 cases show very similar SH and globally averaged responses.

The responses in the annual mean profile in H_2O, NO_y, and ozone at 45°N for to the K_{yy} scenarios are shown in Figure 7, and reveal some complicated behavior. Below the peak level of emission (18 km), the responses in H_2O and NO_y concentration decrease with increasing diffusion, with the opposite occurrence above 20 km. Below 16-18 km at mid-high latitudes of both hemispheres (SH not shown), more material is removed from the stratosphere with larger K_{yy} via cross-tropopause transport. However above ~20 km, the amount of material is directly proportional to K_{yy}, since a larger horizontal diffusion recycles more material throughout the stratosphere before returning to the troposphere. As discussed in Part 1, a similar result was obtained in simulations of mean age in that a larger K_{yy} implies a longer stratospheric residence time, and hence an older mean age. The ozone profile in Figure 7 generally follows this pattern such that below 18 km, the larger responses in NO_y and H_2O with a smaller K_{yy} produce a larger response in ozone. Conversely above 20 km, the scenario with the largest K_{yy} gives the largest ozone response due to the largest enhancements of NO_y and H_2O.

Thus far, we have treated variations in K_{yy} independently of changes in the other transport components. In reality, changes in K_{yy} are due to changes in wave driving which simultaneously affect the residual circulation. To investigate this coupling, we ran an additional scenario (O) in which K_{yy} has been decreased by a factor of 5 as in scenario K, along with a corresponding factor of 5 decrease in the wave drive above the tropopause, which weakens the circulation. The reference and peturbation total ozone fields for this scenario are shown in Figure 8 (top panels). Scenario O simulates a reference total ozone that is similar to the very weak circulation case (B) in Figure 1, but with somewhat stronger gradients due to the smaller K_{yy}. As in scenario K (Figure 6), the perturbation total ozone response for scenario O has a larger hemispheric difference compared to the base case. Additionally, scenario O has an enhanced negative total ozone response at all latitudes compared to the base case, due to the weaker circulation.

Figure 8 (bottom panels) also shows the case with both K_{yy} and wave drive increased by a factor of 5 (scenario P). Here the reference and perturbation total ozone are similar to the very strong circulation (scenario E, Figure 1), with slightly weaker latitudinal gradients. Also, the enhanced circulation in scenario P greatly decreases the negative responses throughout the globe compared to the K_{yy}*5 only case (scenario N, Figure 6).

The rate of horizontal mixing in the tropics has been discussed in previous studies [e.g., *Plumb,* 1996]. Our base model uses a tropical stratospheric K_{yy} field that varies spatially and seasonally, ranging from 10^8 to 10^{10}cm^2/s (see Appendix, Part 1). To test the sensitivity of the HSCT perturbations to the model horizontal diffusion in the tropics, we ran an additional scenario (Q) with K_{yy} set to a very small value of 10^8 cm^2/s in the tropical stratosphere at 15°S-15°N, 15-50 km for all seasons. As seen in Figure 9, the resulting simulations show enhanced tropical and subtropical horizontal gradients compared to the base case, especially in the perturbation total ozone response. While the NH average perturbation is the same as in the base case, the SH and global

average responses are somewhat weaker in this scenario. Note that the SH average response and the large ozone loss simulated in the Antarctic spring have been only *slightly* diminished in this scenario relative to the base case. Consistent with Figure 2, this illustrates that emission products are primarily being transported from the NH to the SH *not* by horizontal diffusive transport through the tropical stratosphere, but by way of the cross-hemispheric transport via the residual circulation in the mesosphere and the subsequent wintertime descent into the lower stratosphere.

As a final K_{yy} sensitivity test, we investigated the model response to changes in horizontal diffusion across the tropopause. Recent assessment reports have noted the importance of cross-tropopause transport in model simulations of HSCT emissions [*Kawa et al.*, 1999; *Park et al.*, 1999]. In our model, there is cross-tropopause transport horizontally via the K_{yy} field where the tropopause height changes with latitude. This occurs primarily at midlatitudes. To test how this horizontal diffusive transport affects the HSCT perturbation in our model, we ran an additional scenario (R) in which the cross-tropopause K_{yy} values were significantly increased over the baseline (see Part 1). However, the reference and perturbation response in total ozone (not shown), and the hemispheric and global mean responses (Table 1) remained virtually unchanged in this scenario relative to the base case. Tracer simulations (Part 1) also changed only very slightly in this case, as did the mean age-NO_y correlation which will be discussed in section 3.8. This illustrates the very small sensitivity to the rate of horizontal cross-tropopause diffusive transport in our model simulations.

3.5. Sensitivity to combined transport changes

In this section we explore how simultaneous changes to the model circulation, K_{yy}, and K_{zz} fields affect the simulated HSCT perturbations. Scenario S combines transport changes which all contribute to a moderately slow emission removal from the stratosphere. These include the weak circulation (scenario C), small lower stratospheric

K_{zz} (scenario F), and moderately large K_{yy} (scenario M). The change in the absolute concentration of H_2O and NO_y in Figure 10 (dashed-triple dotted line) reflects this slow emission removal, which leads to large ozone loss between 18 and 22 km. In this case, the negative total ozone response (Figure 11) is significantly enhanced throughout the globe relative to the base case, and the SH average response is slightly greater than the NH (Table 1).

We also ran a scenario combining the transport changes which contribute to a moderately fast emission removal from the stratosphere (scenario T). These include the strong circulation (scenario D), moderately large K_{zz} (scenario G), and moderately small K_{yy} (scenario L). Figure 10 shows that this fast emission removal scenario (dotted line) simulates significantly weaker ozone loss in the lower stratosphere compared to the base case. In scenario T, the NH high latitude response in total ozone (Figure 11) is similar to the baseline. However at all other latitudes, the response is significantly weaker relative to the base transport, with the NH average response being a factor of 1.5 greater than in the SH.

Similar to the circulation scenarios in Figure 3, combination scenario T gives a smaller absolute ΔNO_y, but gives a larger percentage change relative to the base case near the peak altitude. In fact, the percentage change in NO_y in scenarios S and T are nearly identical. This is due to the decrease in the local background NO_y concentration caused by the faster transport in scenario T. The background concentrations of H_2O have significantly weaker gradients and are much less affected by transport changes, so that the absolute and percentage changes in H_2O have similar dependences on the transport rates.

To test the extreme limits of these sensitivity tests, we combined the transport scenarios which had the very slowest and very fastest stratospheric emission removal rates discussed in this study. Scenario U combines the very weak circulation (scenario B), small K_{zz} (scenario F), and very large K_{yy} (scenario N), with the opposite combination

(scenarios E, H, and K) used for scenario V. These scenarios give reference total ozone and tracer simulations (Part 1) that are even further outside the range of measurements than those simulated by scenarios S and T. The hemispheric and globally averaged total ozone responses are nearly -1% for scenario U, and very close to zero for scenario V (Table 1). The NH average response is actually very slightly positive in scenario V. Scenarios U and V represent the absolute largest and smallest perturbation responses in total ozone that we obtained in this study by varying the advective and diffusive transport rates in our model.

3.6. 1995 model transport

As a final scenario, we ran the HSCT perturbation simulations using the previous 1995 version of our model transport (scenario W). This was used in the 1995 NASA HSCT assessments [*Stolarski et al.,* 1995]. The new 1999 model transport (base scenario A) gives tracer simulations that are in significantly better agreement with observations compared to the previous 1995 transport, as discussed in Part 1 [see also *Fleming et al.,* 1999]. These studies showed that relative to observations and the 1999 model, the 1995 model transport rates are generally too fast, and do not properly resolve the changes in transport across regions that have differing transport characteristics, e.g., changes in vertical mixing across the tropopause. As seen in Figure 10, this results in significantly faster stratospheric removal of H_2O and NO_y, and hence a much weaker annual mean ozone response at 45°N relative to the base scenario.

It is interesting that the reference total ozone simulation with the 1995 transport in Figure 11 is reasonably similar to the 1999 transport (base case), and to climatological TOMS data. However consistent with Figure 10, the perturbation total ozone response is significantly weaker than the 1999 model transport in both hemispheres. The annual and global mean total ozone response is -0.25% in scenario W compared to -0.59% in the base case. This illustrates how model transport deficiencies that are illuminated in inert

in inert tracer simulations can be hidden in chemically active species such as reference total ozone, and can ultimately cause significant biases in the model simulated ozone response to HSCT perturbations.

3.7. Age versus Total ozone perturbation response

The simulations of mean age (Γ) using these different transport scenarions were discussed in Part 1. The correlation of mean age with the total ozone perturbation response for the 23 transport scenarios is shown in Figure 12. Here we plot the global, annual and pressure weighted average of Γ over the 16-22 km region against the global and annual mean perturbation total ozone responses from Table 1. There is a strong correlation between the mean age and total ozone response, such that faster transport rates yield a younger mean age, shorter stratospheric residence time, and less emission accumulation, and result in less ozone loss. As expected, the very slow and very fast emission removal scenarios (S and V) exhibit the extremes in mean age and total ozone perturbation response.

Figure 12 shows that the increasingly negative total ozone response with increasing age appears to asymptote. There is a large change in Γ between scenarios T and S (the combination slow and very slow emission removal cases), but only a small corresponding enhancement of the ozone loss. This suggests that there is an upper limit in the global ozone response caused by increasing the stratospheric residence time. This asymptotic behavior is also seen in the scenarios that have changes in the circulation (A, B, C, D, E), and stratospheric K_{yy} fields (K, L, M, N, Q) separately, especially as seen in the difference between moderate and large K_{yy} increases (scenarios M and N). Scenario V produces an extremely young mean age, and simulates a near zero total ozone response in the global mean. However, it is unclear from the results presented here that shortening the residence time even further would result in a significant positive global mean total ozone response.

3.8. Age versus NO_y accumulation

To test the long term accumulation of NO_y from stratospheric aircraft emissions in our model, we performed an additional experiment corresponding to the "A3" transport run used in the recent Models and Measurements Intercomparison Project II (MMII) [*Park et al.*, 1999]. In this run, NO_y is calculated as a passive tracer except for a specified tropospheric loss, and is run to steady state. The emissions are global, but are input primarily at NH midlatitudes, and correspond to 500 HSCTs at Mach 2.4, with E.I.=10. Figure 13 shows the accumulation of NO_y mass plotted against the pressure-weighted mean age for the 23 transport scenarios used in this study. The values are annually averaged for 35°N-55°N at 24-30 km (top) and 16-22 km (bottom), with the latter corresponding to the altitude range of peak HSCT emission.

As mean age is related to the stratospheric residence time, there is an overall strong correlation between NO_y and Γ at both altitude regions. Faster transport rates imply a younger mean age and a smaller NO_y mass accumulation. The combination very slow and very fast emission removal scenarios (U and V) exhibit the extremes in both quantities throughout the stratosphere (note that scenario U, with a mean age of 8.4 years and a NO_y accumulation of 4.9×10^8 kg, is off the scale in the bottom panel in Figure 13).

In the middle stratosphere (24-30 km), it appears that transport processes affect mean age and NO_y accumulation in a similar fashion, as the NO_y-Γ correlation is tightly compact and almost completely linear. However at 16-22 km, the correlation is more scattered and depends on the type of transport variation imposed. For example, the circulation scenarios (A, B, C, D, E) show a strong linear correlation, as do the minimum lower stratospheric K_{zz} scenarios (A, F, G, H). However, variations in stratospheric K_{yy} (scenarios A, K, L, M, N, Q) show a much weaker NO_y-Γ correlation. It appears that while large scale increases in K_{yy} strongly increase the mean age globally at 16-22 km by recycling more air throughout the stratosphere, the corresponding change in NO_y

accumulation is quite small. Changes in the strength of the mesospheric gravity wave effects (scenarios A, I, and J) also show a similar NO_y-Γ correlation. Changing the gravity wave strength strongly affects the circulation and vertical diffusion in the upper stratosphere and mesosphere (see section 3.3 in the companion paper). The resulting mean age at 16-22 km ranges from 2.8 to 3.2 years in scenarios I and J, whereas the corresponding change in NO_y accumulation is negligible.

The MMII analysis [*Park et al.*, 1999] showed that the relationship between mean age and NO_y accumulation at 16-22 km exhibited a stronger correlation in 2-D than in 3-D models. The weak correlation simulated in our model K_{yy} scenarios and gravity wave scenarios shown in Figure 13 (bottom) is similar to the NO_y-Γ correlation pattern simulated by the 3-D models in the MMII analysis. The MMII analysis also suggests that perhaps the fundamentally different formulations of troposphere-stratosphere exchange processes in 2-D and 3-D models result in different NO_y-Γ correlation patterns.

To examine the influence of the horizontal cross-tropopause diffusive transport in our 2-D model, we can compare results from the base case and scenario R, in which K_{yy} was significantly increased in regions where the tropopause height changes with latitude (see section 3.4). Figure 13 shows that scenario R exhibited only small changes, relative to scenario A, in both NO_y accumulation and Γ at both altitude regions. Furthermore, the changes in NO_y and age are strongly correlated in this scenario, unlike the other K_{yy} scenarios (K, L, M, N, Q) discussed above. Therefore, it appears that horizontal cross-tropopause diffusive transport has little influence on our model simulations.

4. Conclusions

In this study, we have examined how simulations of stratospheric aircraft perturbations are affected by variations in 2-D model transport fields. The resulting HSCT responses in H_2O, NO_y, and ozone are generally consistent with the mean age and tracer simulations reported in Part 1 of this study. As a result, there is a strong

correlation between mean age and the total ozone perturbation simulated by the various transport scenarios.

Changes to the strength of the residual circulation in the upper troposphere and stratosphere had an effect similar to changing the lower stratospheric K_{zz} values: increasing the transport rates increases the rate of removal of material from the stratosphere, thereby decreasing the residence time of the HSCT emissions, and producing a less negative ozone response. Increasing the stratospheric horizontal diffusion generally enhanced the hemispheric and globally averaged total ozone perturbation response, while decreasing the associated latitudinal gradients. This is consistent with the fact that the overall stratospheric mean age, and hence the emission residence time increases with increasing K_{yy} as discussed in Part 1. Simulations with very small tropical stratospheric K_{yy} resulted in a slightly smaller negative SH and globally averaged total ozone response, with no change in the NH response, compared to the base case. Significant variations in the strength of the mesospheric gravity wave drag and diffusion strongly influenced tracers in the mesosphere as reported in Part 1, but caused only very minor changes in the lower stratospheric HSCT response compared to the base case.

Incorporating K_{yy} changes along with self-consistent changes in the corresponding planetary wave drive, and hence, the residual circulation, had a cancellation effect, and produced a significantly different HSCT response compared to changing only the K_{yy} rates. For example, while increasing K_{yy} globally increases the stratospheric residence time of the emission and enhances the negative total ozone response, also including a stronger wave drive, and hence, an enhanced circulation implied by the larger K_{yy} decreases the overall residence time and produces a weaker negative ozone response.

As reported in Part 1, the base model transport provided the most favorable overall comparison with a variety of tracer observations. This scenario simulated a global/annual mean total ozone response of -0.59%, with only a slightly larger response

in the NH compared to the SH. The shortest stratospheric residence time and weakest total ozone response was simulated by combining a strong circulation, large lower stratospheric K_{zz}, and small K_{yy} field. Conversely, combining a weak circulation, small lower stratospheric K_{zz}, and a large stratospheric K_{yy} field yielded the largest negative response. For transport scenarios which gave tracer simulations within some agreement with measurements, the annual/globally averaged total ozone response ranged from -0.45% to -0.70%. The absolute upper and lower limits of the annual/globally averaged response in total ozone obtained in this study ranged from near zero to slightly less that -1%. However, the associated transport rates in these scenarios resulted in tracer simulations that were far outside the range of observations.

An important aspect of modeling the response to HSCT perturbations is to properly represent the distribution and long term accumulation of aircraft exhaust. As mean age and stratospheric residence time are related, the model transport simulations of passive NO_y accumulation and mean age revealed an overall strong correlation throughout the stratosphere. Faster transport rates resulted in a younger mean age and a smaller NO_y mass accumulation. In the middle stratosphere, changes in NO_y and Γ were similar and tightly correlated among all the different transport variations imposed. In the lower stratosphere, circulation and K_{zz} changes also produced a strong correlation, while variations in K_{yy} and mesospheric gravity wave strength resulted in changes in mean age, but only very slight or negligible changes in NO_y accumulation. This weak correlation among the K_{yy} scenarios is similar to 3-D model simulations performed in the MMII ananlysis, We also note that our model simulated NO_y-Γ correlation and HSCT perturbation in the stratosphere showed only very small sensitivity to the magnitude of the horizontal diffusive transport across the tropopause.

As a final note, it is interesting that our previous 1995 model transport simulates a reference total ozone field that is reasonably similar to the 1999 base model and to climatological TOMS data. However as discussed in Part 1, our 1999 model transport

gives tracer simulations that are in significantly better agreement with measurements compared to the 1995 transport. This previous version exhibited overly fast transport rates in all of the model-measurement tracer comparisons, and simulated annual/global mean ages that were 40-60% younger throughout the stratosphere compared with the 1999 transport. As a result, the 1995 model gives a weaker HSCT perturbation total ozone response compared to the 1999 model, with annual/globally averaged values of -0.25% and -0.59%, respectively. This illustrates that model transport deficiencies, which are evident in inert tracer comparisons, can be hidden in chemically active constituents such as reference total ozone, and can ultimately cause significant biases in the simulated HSCT perturbation ozone response.

Acknowledgments. We thank the NASA Atmospheric Chemistry Modeling and Analysis Program and the UARS Science Investigation Program for support of this project.

References

DeMore, W.B., S.P. Sander, D.M. Golden, R.F. Hampson, M.J. Kurylo, C.J. Howard, A.R. Ravishankara, C.E. Kolb, and M.J. Molina, Chemical kinetics and photochemical data for use in stratospheric modeling, Evaluation number 12, *JPL Publ., 97-4*, 266 pp., 1997.

Douglass, A.R., C.H. Jackman, R.S. Stolarski, Comparison of model results transporting the odd nitrogen family with results transporting separate odd nitrogen species, *J. Geophys. Res., 94*, 9862-9872, 1989.

Fleming, E.L., C.H. Jackman, R.S. Stolarski, and D.B. Considine, Simulation of stratospheric tracers using an improved empirically-based two-dimensional model transport formulation, *J. Geophys. Res.*, (in press), 1999.

Garcia, R.R., and S. Solomon, A numerical model of the zonally averaged dynamical and chemical structure of the middle atmosphere, *J. Geophys. Res., 88*, 1379-1400, 1983.

Garcia, R.R., F. Stordal, S. Solomon, and J.T. Kiehl, A new numerical model of the middle atmosphere, 1. Dynamics and transport of tropospheric source gases, *J. Geophys. Res., 97*, 12967-12991, 1992.

Hall, T.M., and D.W. Waugh, Tracer transport in the tropical stratospheric due to vertical diffusion and horizontal mixing, *Geophys. Res. Lett., 24*, 1383-1386, 1997.

Inter-governmental Panel on Climate Change (IPCC), *Special Report on Aviation and the Global Atmosphere*, 1999.

Jackman, C.H., A.R. Douglass, R.B. Rood, R.D. McPeters, and P.E. Meade, Effect of solar proton events on the middle atmosphere during the past two solar cycles as computed using a two-dimesional model, *J. Geophys. Res., 95*, 7417-7428, 1990.

Jackman, C.H., A.R. Douglass, K.F. Brueske, and S.A. Klein, The influence of dynamics on two-dimensional model results: Simulations of ^{14}C and stratospheric NO_x injections, *J. Geophys. Res., 96*, 22559-22572, 1991.

Jackman, C.H., E.L. Fleming, S. Chandra, D.B. Considine, and J.E. Rosenfield, Past, present, and future modeled ozone trends with comparisons to observed trends, *J. Geophys.*

Res., 101, 28753-28767, 1996.

Kawa, S. R. et al., Editors, Assessment of the Effects of High Speed Aircraft in the Stratosphere: 1998, *NASA Reference Publication NASA/TM-1999-209237*, 1999.

Kinnison, D. E., H. S. Johnston, H. S., and D.J. Wuebbles, Model study of atmospheric transport using carbon 14 and strontium 90 data as inert tracers, *J. Geophys. Res., 99*, 20647-20664, 1994.

Mote, P.W., T.J. Dunkerton, M.E. McIntyre, E.A. Ray, P.H. Haynes, and J.M. Russell III, Vertical velocity, vertical diffusion, and dilution by midlatitude air in the tropical lower stratosphere, *J. Geophys. Res., 103*, 8651-8666, 1998.

Park, J. H., M. K. W. Ko, C. H. Jackman, and R. A. Plumb, Editors, Report of the 1997 Models and Measurements Workshop, held November 3-5, 1997, Williamsburg, Virginia, *NASA Reference Publication XXXX*, 1999.

Plumb, R.A., A "tropical pipe" model of stratospheric transport, *J. Geophys. Res., 101*, 3957-3972, 1996.

Rosenfield, J.E., D.B. Considine, P.E. Meade, J.T. Bacmeister, C.H. Jackman, and M.R. Schoeberl, Stratospheric effects of Mount Pinatubo aerosol studied with a coupled two-dimensional model, *J. Geophys. Res., 102*, 3649-3670, 1997.

Stolarski, R.S., et al., Scientific assessment of the atmospheric effects of stratospheric aircraft, *NASA Ref. Pub., 1381*, 110 pp., 1995.

Weisenstein, D.W., M.K.W. Ko, J.M. Rodriguez, and N.D. Sze, Impact of heterogeneous chemistry on model-calculated ozone change due to HSCT aircraft, *Geophys. Res. Lett., 18*, 1991-1994, 1991.

Weisenstein, D.W., M.K.W. Ko, N.D. Sze, and J.M. Rodriguez, Potential impact of SO_2 emissions from stratospheric aircraft on ozone, *Geophys. Res. Lett., 23*, 161-164, 1996.

World Meteorological Organization (WMO), Scientific Assessment of Ozone Depletion: 1998, *Rep. 44* Global Ozone Research and Monitoring Project, Geneva, 1999.

This manuscript was prepared with the AGU LaTeX macros v3.0.

Figure Captions

Figure 1. Season-latitude cross sections of reference total ozone in Dobson units (DU) (left hand column), and the perturbation response (% change, subsonics+supersonics minus subsonics only) in total ozone (right hand column) for the base scenario A and the four circulation scenarios as listed in Table 1: very weak circulation (B); weak circulation (C); strong circulation (D); and the very strong circulation (E). Contour intervals are 30 DU for the left hand column. For the right hand column, contour intervals are .5% for values less (more negative) than -2%, and .2% including the -.1% contour for values greater (more positive) than -2%.

Figure 2. Time-latitude sections of carbon 14 for the three altitudes indicated. Values are in mixing ratio units, defined as 10^5 atoms of ^{14}C per gram of dry air [*Kinnison et al.*, 1994]. Contour intervals are 50, including the 60 contour, for values less than 500, and 100 for values greater than 500.

Figure 3. Vertical profiles of the perturbation response (subsonics+supersonics minus subsonics only) in the model simulated H_2O, NO_y, and ozone from the circulations scenarios as discussed in the text. Shown are the very weak circulation (B, dashed-triple dotted line); weak circulation (C, dashed line); strong circulation (D, dashed-dotted line); very strong circulation (E, dotted line); and the base case (A, solid line). Included are the percentage change (left-hand column) and the change in concentration (right-hand column).

Figure 4. Season-latitude cross sections of reference total ozone in Dobson units (DU) (left hand column), and the perturbation response (% change, subsonics+supersonics minus subsonics only) in total ozone (right hand column) for the base scenario A and the three stratospheric K_{zz} scenarios as listed in Table 1: minimum K_{zz}=0.001 m^2/s (F), minimum K_{zz}=0.1 m^2/s (G), and minimum K_{zz}=1 m^2/s (H). Contour intervals are 30 DU for the left hand column. For the right hand column, contour intervals are .5% for values less (more negative) than -2%, and .2% including the -.1% contour for values greater (more positive) than -2%.

Figure 5. Vertical profiles of the perturbation response (subsonics+supersonics minus subsonics only) in the model simulated H_2O, NO_y, and ozone from the stratospheic K_{zz} scenarios as discussed in the text. Shown are: minimum K_{zz}=0.001 m^2/s (F, dashed-triple dotted line); minimum K_{zz}=0.1 m^2/s (G, dashed line); minimum K_{zz}=1 m^2/s (H, dotted line); and the base case (A, solid line). Included are the percentage change (left-hand column) and the change in concentration (right-hand column).

Figure 6. Season-latitude cross sections of reference total ozone in Dobson units (DU) (left hand column), and the perturbation response (% change, subsonics+supersonics minus subsonics only) in total ozone (right hand column) for the base scenario A and four stratospheric K_{yy} scenarios as listed in Table 1: K_{yy} decreased by a factor of 5 (K), K_{yy} decreased by a factor of 2 (L), K_{yy} increased by a factor of 2 (M), and K_{yy} increased by a factor of 5 (N). Changes to K_{yy} are made only above the tropopause. Contour intervals are 30 DU for the left hand column. For the right hand column, contour intervals are .5% for values less (more negative) than -2%, and .2% including the -.1% contour for values greater (more positive) than -2%.

Figure 7. Vertical profiles of the perturbation response (subsonics+supersonics minus subsonics only) in the model simulated H_2O, NO_y, and ozone from the stratospheic K_{yy} scenarios as discussed in the text. Shown are: K_{yy} decreased by a factor of 5 (K, dashed-triple dotted line), K_{yy} decreased by a factor of 2 (L, dashed line), K_{yy} increased by a factor of 2 (M, dashed-dotted line), K_{yy} increased by a factor of 5 (N, dotted line), and the base case (A, solid line). Included are the percentage change (left-hand column) and the change in concentration (right-hand column).

Figure 8. Season-latitude cross sections of reference total ozone in Dobson units (DU) (left hand column), and the perturbation response (% change, subsonics+supersonics minus subsonics only) in total ozone (right hand column) for the base scenario A and four stratospheric K_{yy} scenarios as listed in Table 1: K_{yy} decreased by a factor of 5 (K, identical to Figure 6), both K_{yy} and the corresponding wave drive decreased by a factor of 5 (O), K_{yy} increased by a factor of 5 (M, identical to Figure 6), and both K_{yy} and the corresponding wave drive increased by a factor of 5 (P). Changes in K_{yy} and wave drive are made only above the tropopause. Contour intervals are 30 DU for the left hand column. For the right hand column, contour intervals are .5% for values less (more negative) than -2%, and .2% including the -.1% contour for values greater (more positive) than -2%.

Figure 9. Season-latitude cross sections of reference total ozone in Dobson units (DU) (top), and the perturbation response (% change, subsonics+supersonics minus subsonics only) in total ozone (bottom) for the very small tropical stratospheric K_{yy} scenario (Q) as discussed in the text. Contour intervals are 30 DU for the left hand column. For the right hand column, contour intervals are .5% for values less (more negative) than -2%, and .2% including the -.1% contour for values greater (more positive) than -2%.

Figure 10. Vertical profiles of the perturbation response (subsonics+supersonics minus subsonics only) in the model simulated H_2O, NO_y, and ozone from: the combination transport scenario S (dashed-triple dotted line), the combination transport scenario T (dotted line), the 1995 transport scenario W (dashed line), and the base case (A, solid line). Included are the percentage change (left-hand column) and the change in concentration (right-hand column). See text and Table 1 for details.

Figure 11. Season-latitude cross sections of reference total ozone in Dobson units (DU) (left hand column), and the perturbation response (% change, subsonics+supersonics minus subsonics only) in total ozone (right hand column) for the base scenario A, the combination transport scenarios S and T, and the 1995 transport scenario W. Contour intervals are 30 DU for the left hand column. For the right hand column, contour intervals are .5% for values less (more negative) than -2%, and .2% including the -.1% contour for values greater (more positive) than -2%.

Figure 12. Scatter plots of the annual and globally averaged perturbation response in total ozone (% change, subsonics+supersonics minus subsonics only), versus the annual, global and pressure weighted average mean age (years) for 16-22 km, for each of the 23 transport scenarios listed in Table 1. Letters for each scenario are color coded according to the type of transport variation imposed, as indicated in the legend.

Figure 13. Scatter plots of mean age (years) versus the accumulation of NO_y mass (in 10^8 kg) from the passive NO_y experiment, for each of the 23 transport scenarios listed in Table 1. Letters for each scenario are color coded according to the type of transport variation imposed, as indicated in the legend. All values are annually averaged and area weighted over 35°N-55°N, for 24-30 km (top), and 16-22 km (bottom). The mean age has been pressure weighted over the altitude range indicated. See text for details. Note that in the bottom panel, scenario U is off the scale with a mean age of 8.4 years and a NO_y accumulation of 4.9×10^8 kg).

Table 1. Percentage change in the hemispheric and globally averaged annual mean perturbation response in total column ozone for each transport scenario as discussed in the text.

Scenario	Description	NH	SH	Global
A	Base (1999 model)	-.60	-.57	-.59
B	very weak trop/strat circulation	-.80	-.61	-.71
C	weak trop/strat circulation	-.72	-.57	-.65
D	strong trop/strat circulation	-.49	-.50	-.50
E	very strong trop/strat circulation	-.31	-.30	-.31
F	stratospheric minimum K_{zz} = .001 m^2/s	-.67	-.67	-.67
G	stratospheric minimum K_{zz} = .1 m^2/s	-.50	-.38	-.45
H	stratospheric minimum K_{zz} = 1 m^2/s	-.12	-.06	-.09
I	weak mesospheric gravity wave drag, K_{zz}	-.61	-.59	-.60
J	strong mesospheric gravity wave drag, K_{zz}	-.58	-.51	-.54
K	$K_{yy}/5$ (above tropopause)	-.56	-.29	-.43
L	$K_{yy}/2$ (above tropopause)	-.63	-.45	-.55
M	K_{yy}*2 (above tropopause)	-.62	-.78	-.70
N	K_{yy}*5 (above tropopause)	-.64	-.76	-.70
O	$K_{yy}/5$ + wave drive/5 (above tropopause)	-.86	-.43	-.66
P	K_{yy}*5 + wave drive*5 (above tropopause)	-.35	-.31	-.33
Q	small tropical stratospheric K_{yy}	-.60	-.47	-.54
R	large cross-tropopause K_{yy}	-.60	-.57	-.58
S	combination, very slow emission removal (B+F+N)	-.90	-.95	-.93
T	combination, slow emission removal (C+F+M)	-.83	-.90	-.86
U	combination, fast emission removal (D+G+L)	-.38	-.25	-.32
V	combination, very fast emission removal (E+H+K)	+.006	-.01	-.001
W	1995 model	-.27	-.22	-.25

FIG 1

linear -4 → -.08

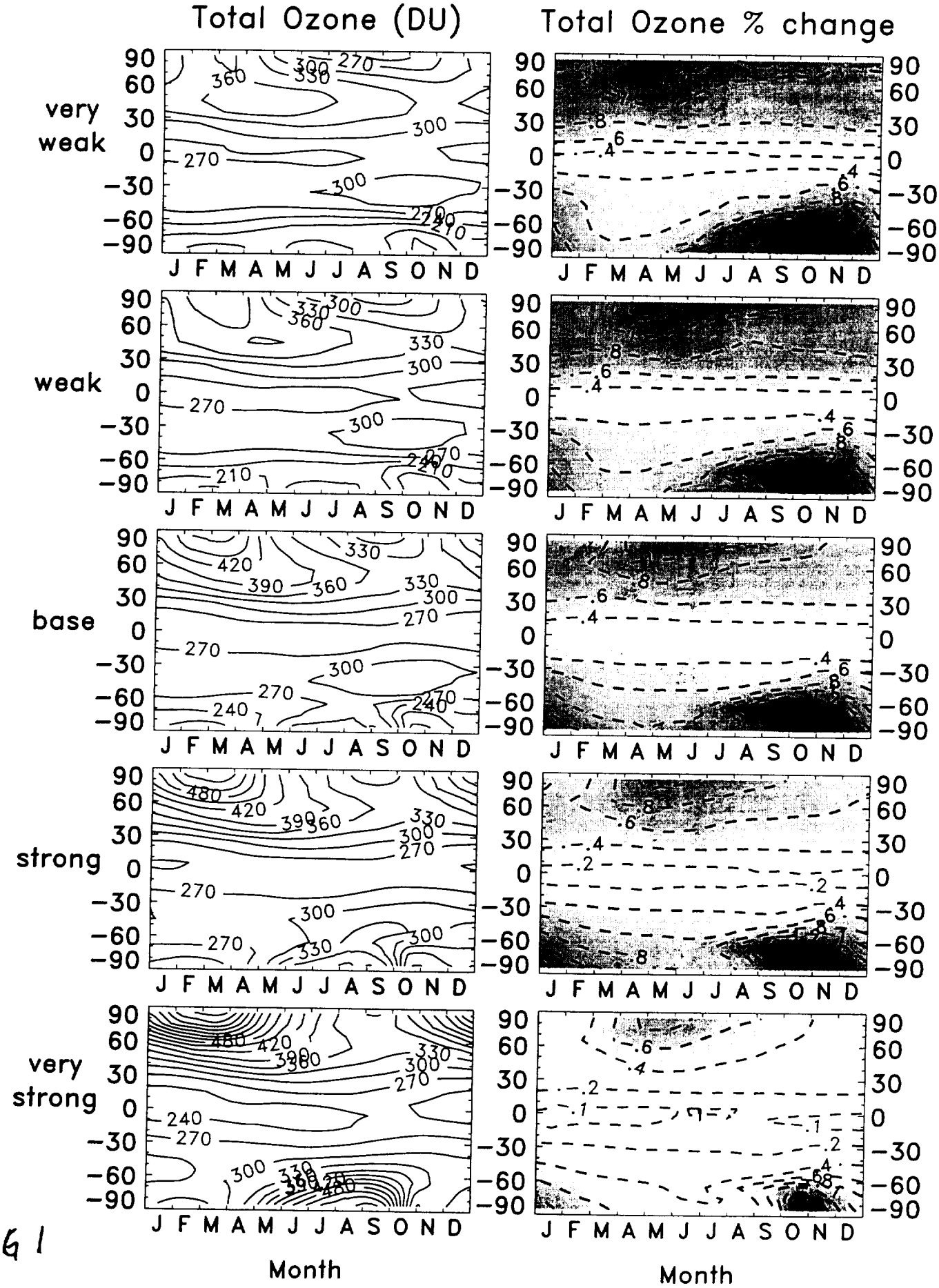

FIG 1

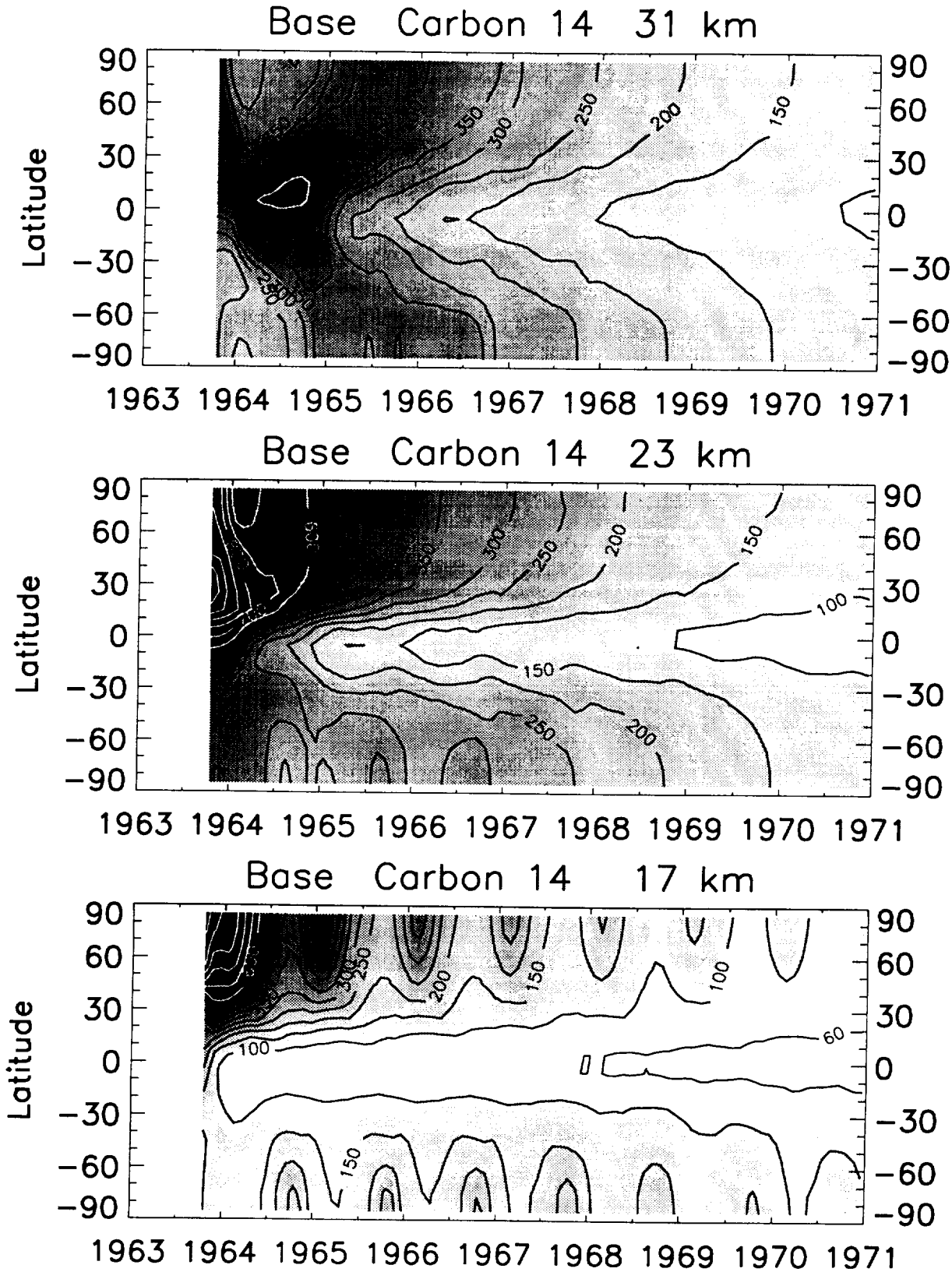
Base Carbon 14 31 km
Latitude
90
60
30
0
−30
−60
−90
350
300
250
200
150
1963 1964 1965 1966 1967 1968 1969 1970 1971
Base Carbon 14 23 km
Latitude
350
300
250
200
150
100
150
250
200
Base Carbon 14 17 km
Latitude
350
300
250
200
150
100
60
100
150

Fig 2

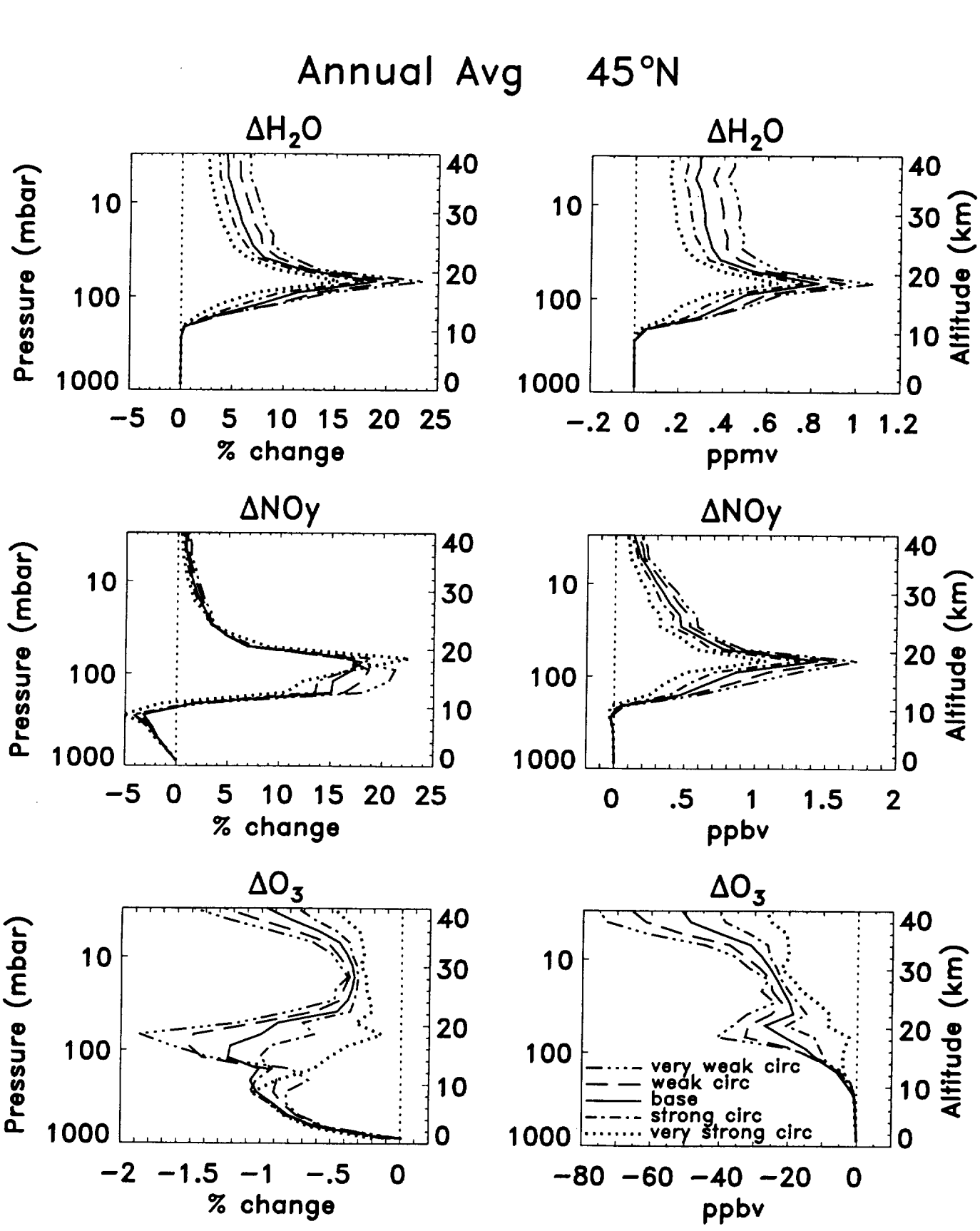
Annual Avg 45°N
ΔH2O
Pressure (mbar)
10
100
1000
40
30
20
10
0
−5 0 5 10 15 20 25
% change
ΔH2O
−.2 0 .2 .4 .6 .8 1 1.2
ppmv
Altitude (km)
ΔNOy
0 .5 1 1.5 2
ppbv
ΔO3
−2 −1.5 −1 −.5 0
−80 −60 −40 −20 0
very weak circ
weak circ
base
strong circ
very strong circ

Fig 3

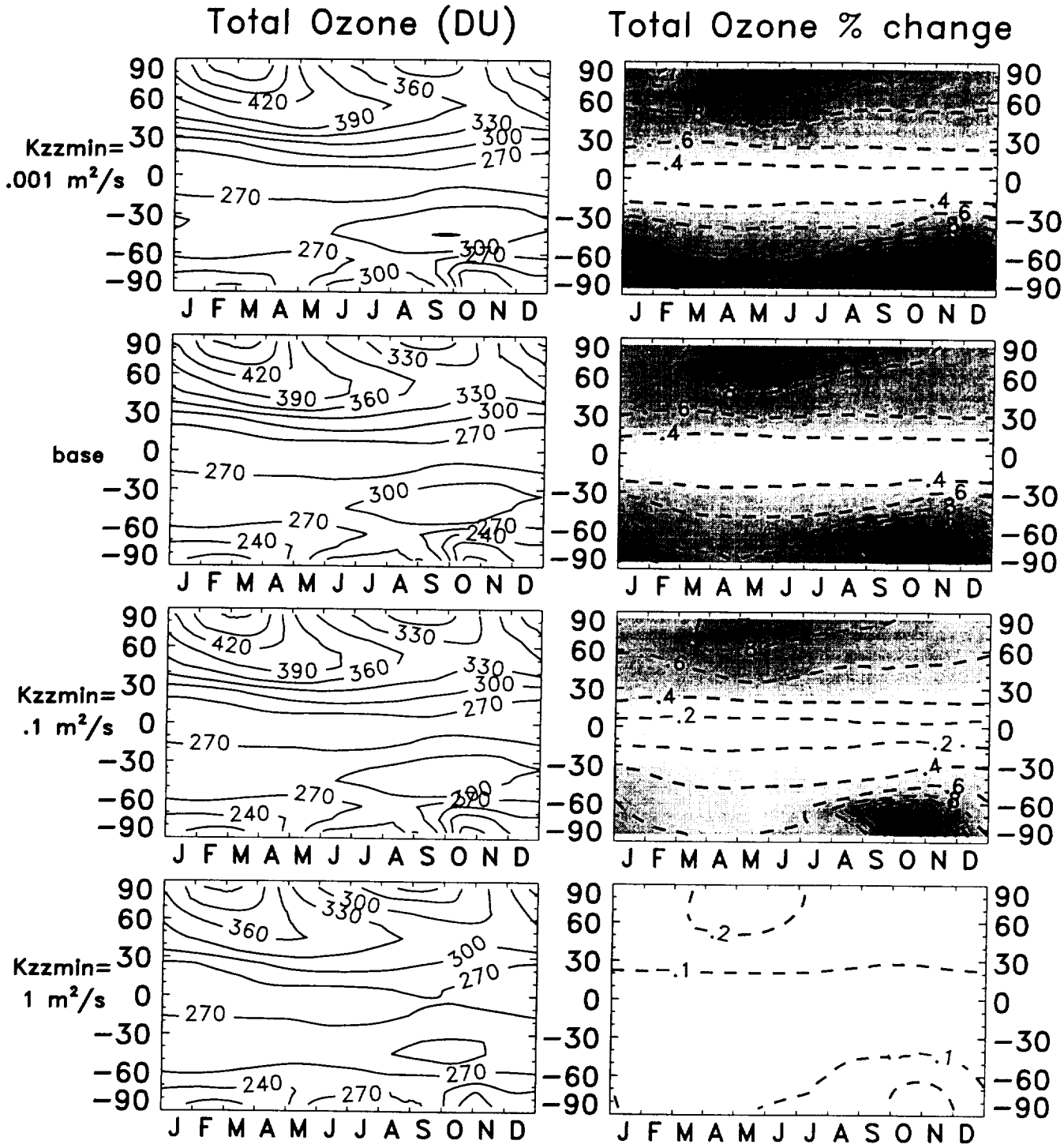
Total Ozone (DU)
Total Ozone % change
Kzzmin= .001 m²/s
base
Kzzmin= .1 m²/s
Kzzmin= 1 m²/s
90
60
30
0
−30
−60
−90
J F M A M J J A S O N D
420
390
360
330
300
270
240
.6
.4
.2
.1

Fig 4

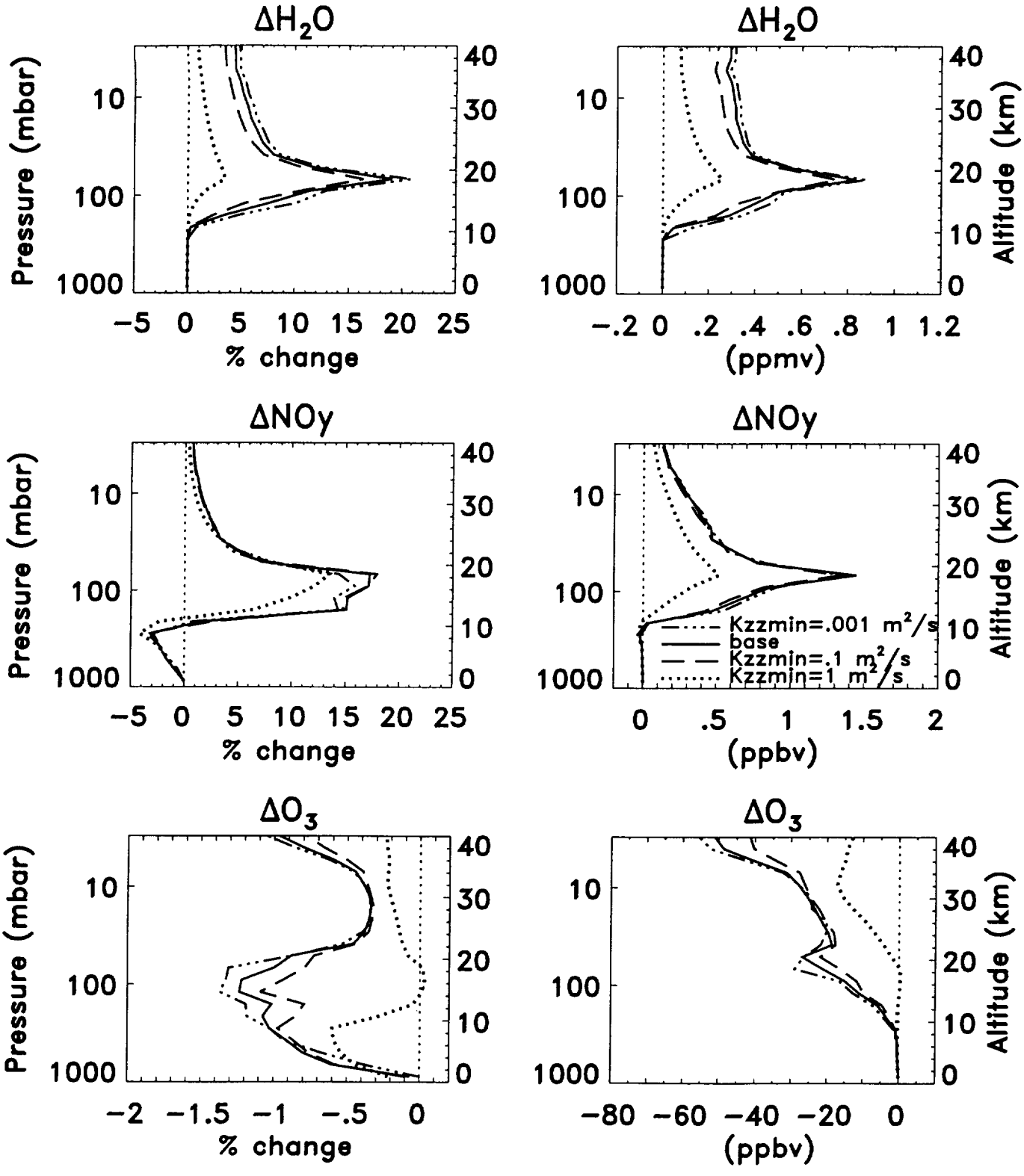
Annual Avg 45°N
ΔH2O
Pressure (mbar)
10
100
1000
40
30
20
10
0
−5 0 5 10 15 20 25
% change
ΔH2O
−.2 0 .2 .4 .6 .8 1 1.2
(ppmv)
Altitude (km)
ΔNOy
−5 0 5 10 15 20 25
% change
ΔNOy
0 .5 1 1.5 2
(ppbv)
Kzzmin=.001 m²/s
base
Kzzmin=.1 m²/s
Kzzmin=1 m²/s
ΔO3
−2 −1.5 −1 −.5 0
% change
ΔO3
−80 −60 −40 −20 0
(ppbv)

Fig 5

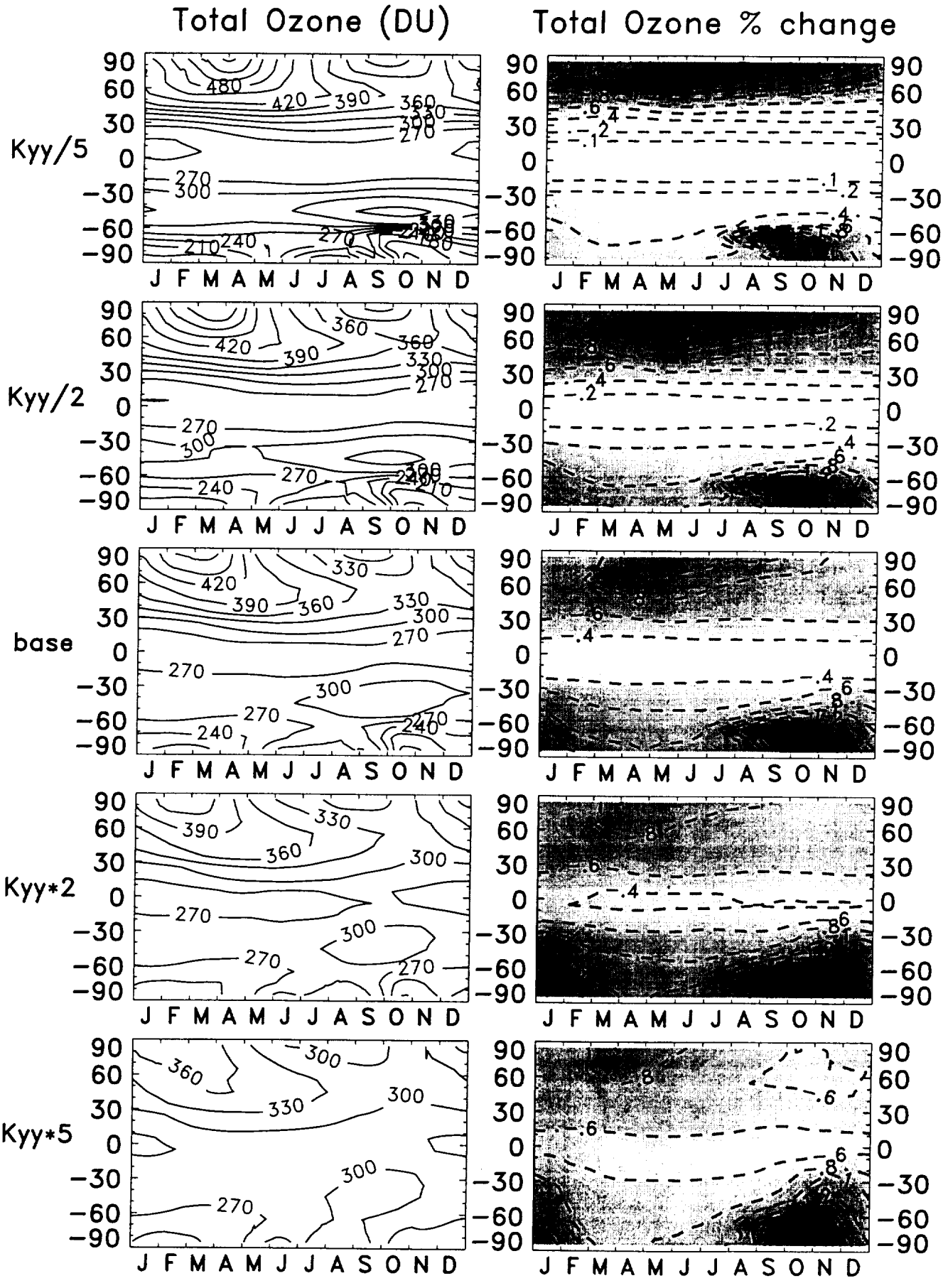
Total Ozone (DU)
Total Ozone % change
Kyy/5
Kyy/2
base
Kyy*2
Kyy*5
90
60
30
0
-30
-60
-90
J F M A M J J A S O N D
Month
Month

Fig 6

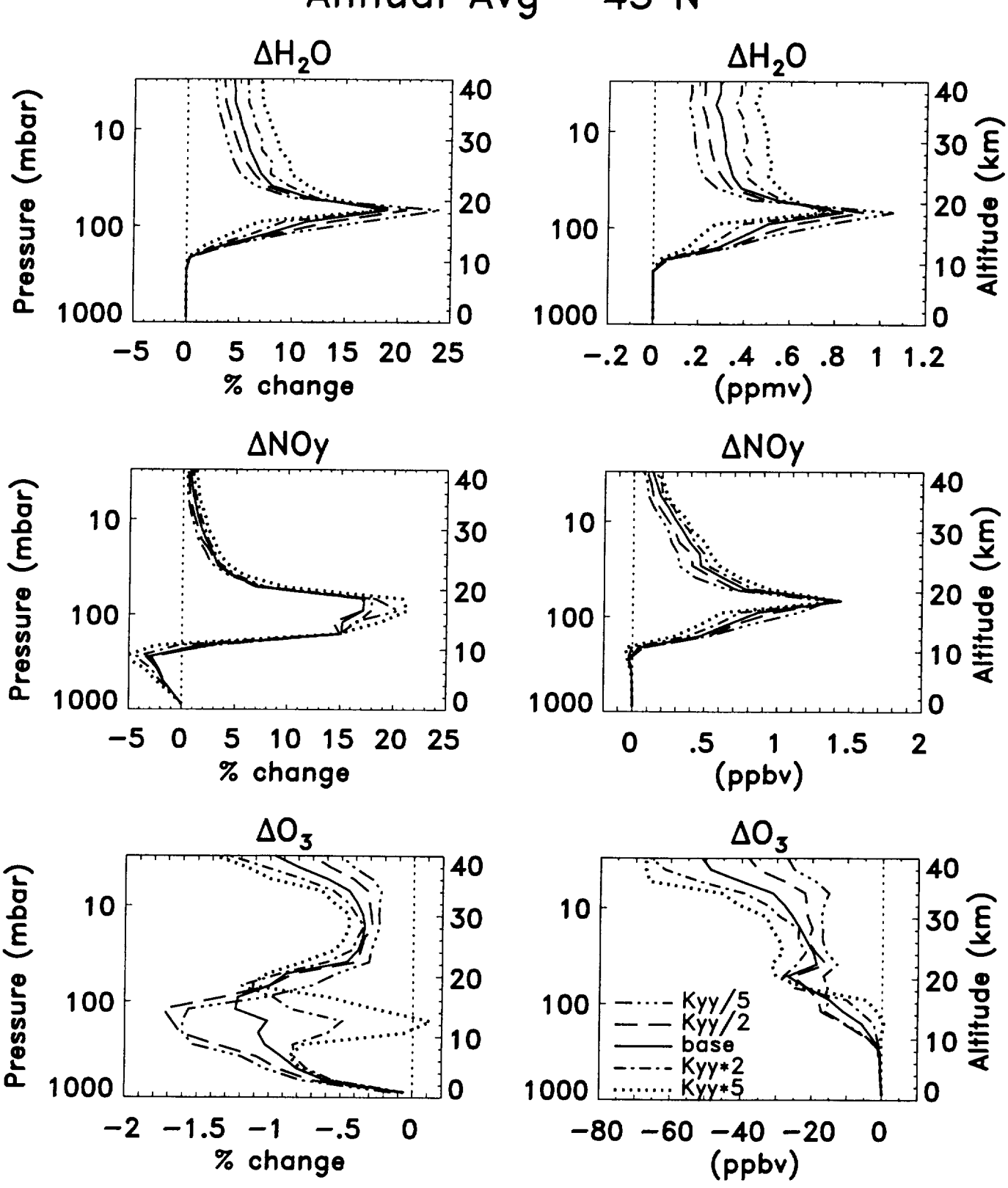
Annual Avg 45°N
ΔH2O
Pressure (mbar)
10
100
1000
40
30
20
10
0
−5 0 5 10 15 20 25
% change
ΔH2O
−.2 0 .2 .4 .6 .8 1 1.2
(ppmv)
Altitude (km)
ΔNOy
0 .5 1 1.5 2
(ppbv)
ΔO3
−2 −1.5 −1 −.5 0
−80 −60 −40 −20 0
Kyy/5
Kyy/2
base
Kyy*2
Kyy*5

Fig 7

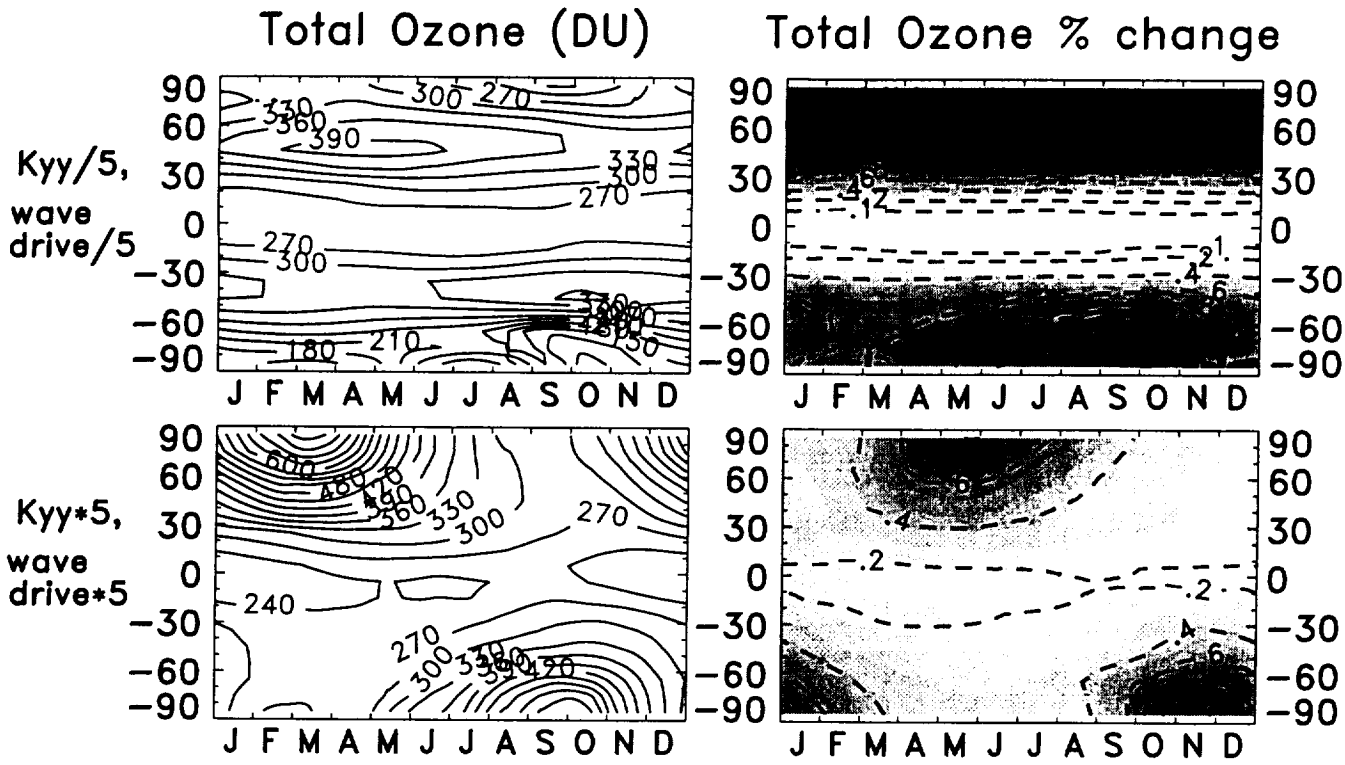
Total Ozone (DU)
Total Ozone % change
Kyy/5,
wave
drive/5
Kyy*5,
wave
drive*5
90
60
30
0
−30
−60
−90
J F M A M J J A S O N D
330
300
270
360
390
240
210
180

FIGURE 8

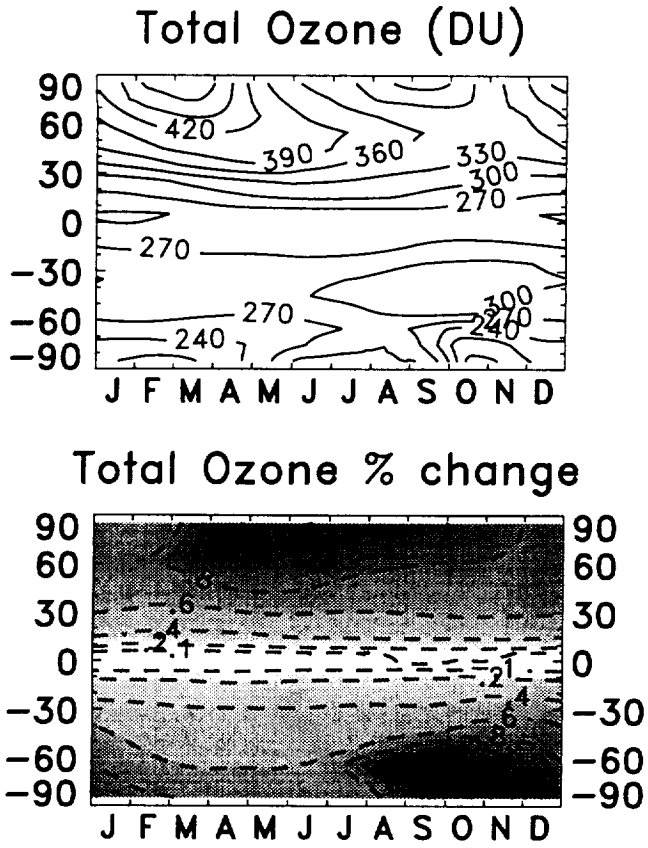
Total Ozone (DU)
90
60
30
0
-30
-60
-90
420
390
360
330
300
270
270
270
300
270
240
240
J F M A M J J A S O N D
Total Ozone % change
90
60
30
0
-30
-60
-90
.8
.6
.4
.2
.1
.1
.2
.4
.6
.8
J F M A M J J A S O N D

Fig. 9

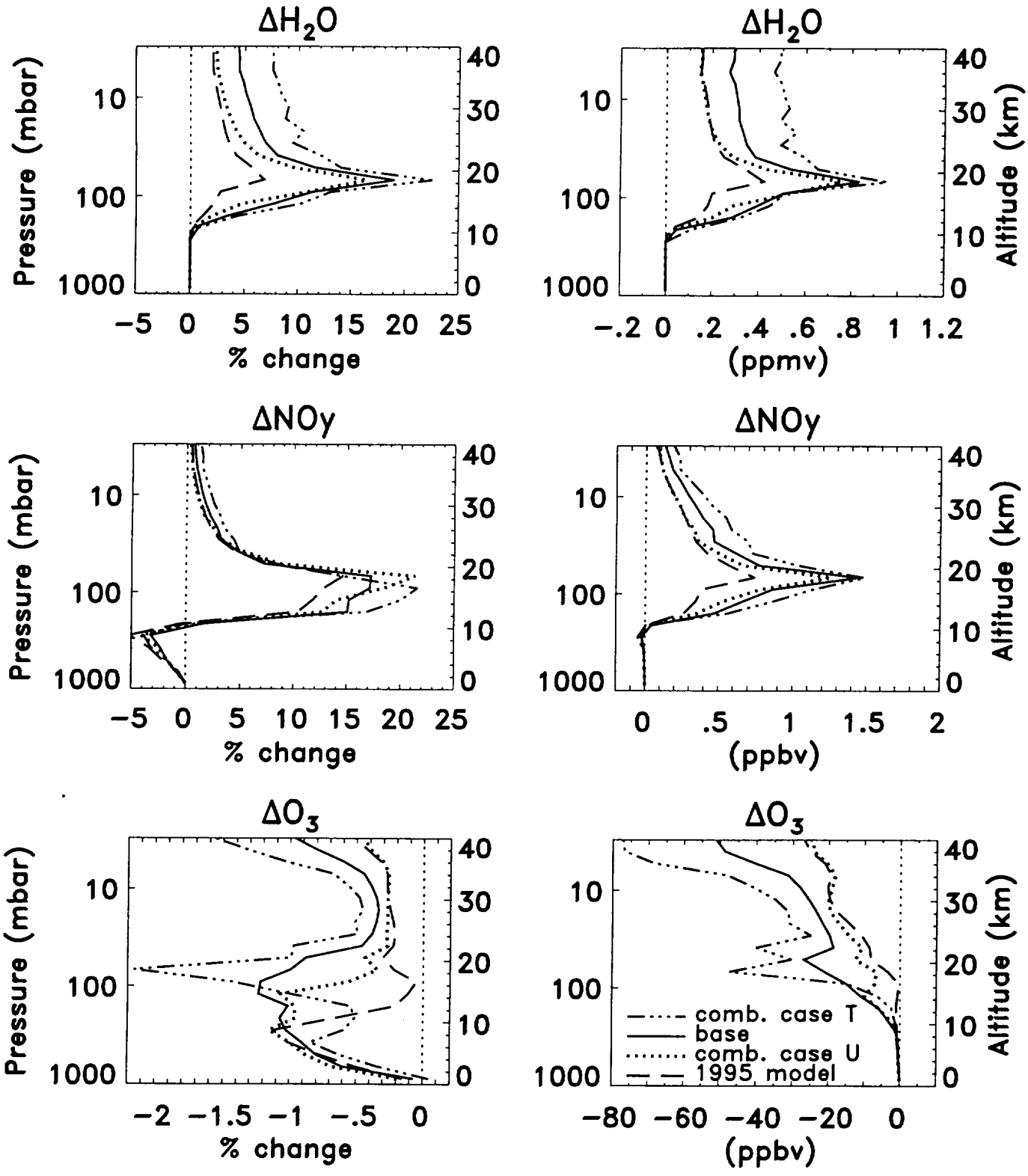
Annual Avg 45°N
ΔH2O
Pressure (mbar)
10
100
1000
40
30
20
10
0
−5 0 5 10 15 20 25
% change
ΔH2O
−.2 0 .2 .4 .6 .8 1 1.2
(ppmv)
Altitude (km)
ΔNOy
% change
ΔNOy
0 .5 1 1.5 2
(ppbv)
ΔO3
−2 −1.5 −1 −.5 0
% change
ΔO3
comb. case T
base
comb. case U
1995 model
−80 −60 −40 −20 0
(ppbv)

FIG. 10

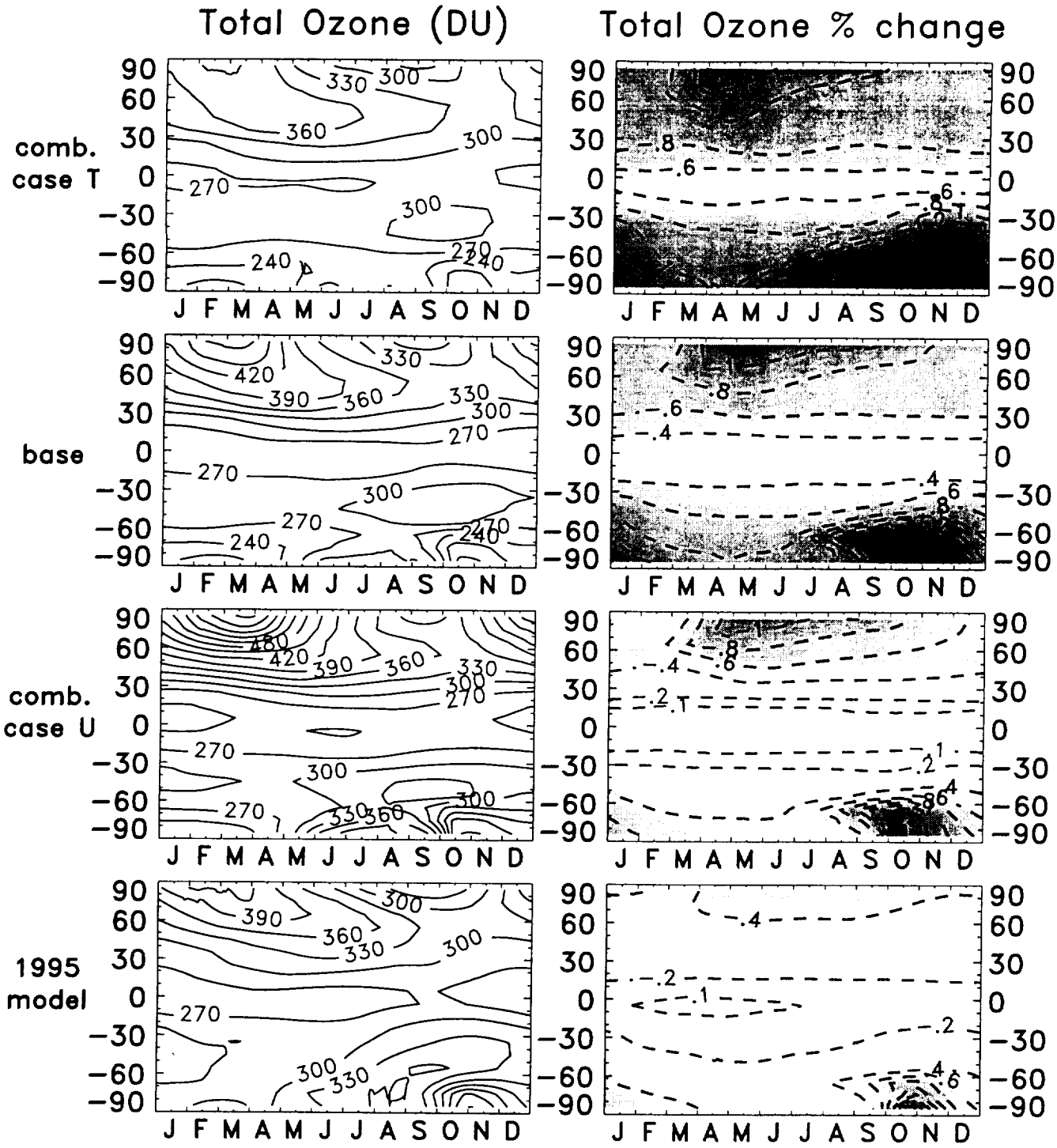
Total Ozone (DU)
Total Ozone % change
comb. case T
base
comb. case U
1995 model
90
60
30
0
−30
−60
−90
J F M A M J J A S O N D
330
300
360
270
240
420
390
480
.8
.6
.4
.2
.1

FIG. 11

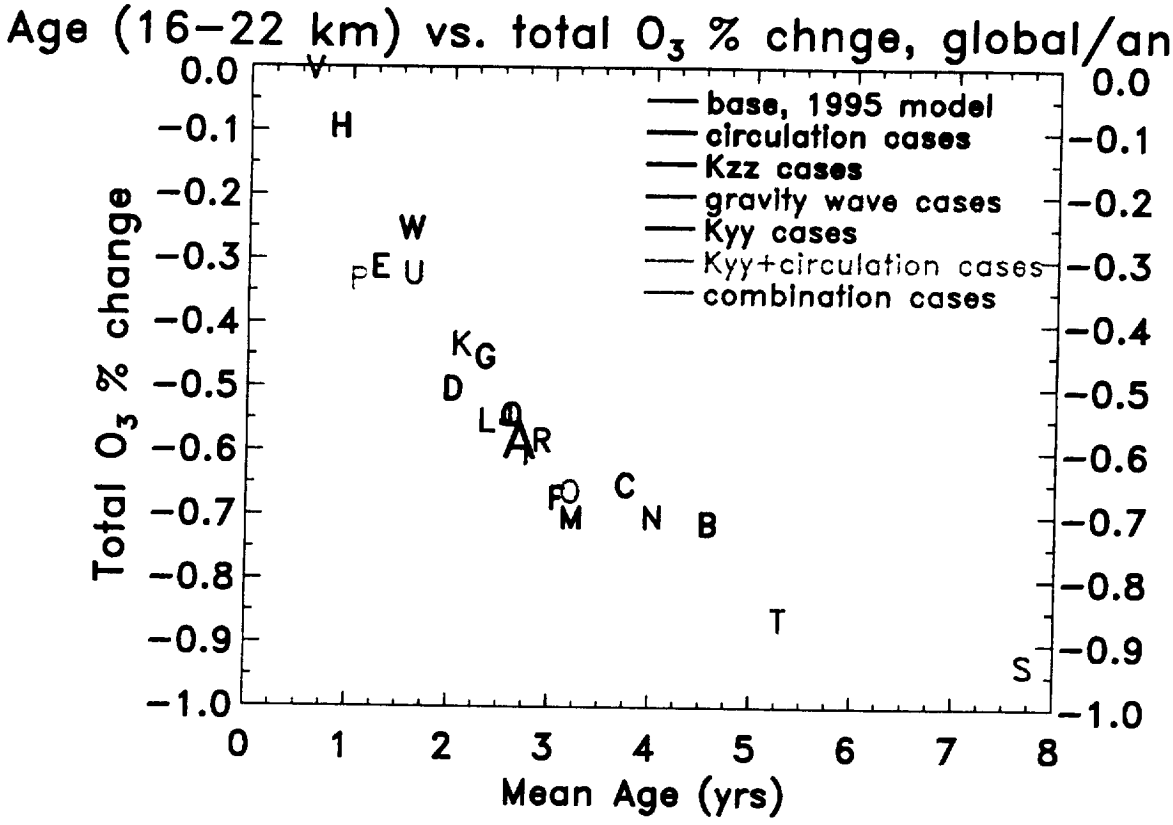
Age (16–22 km) vs. total O_3 % chnge, global/ann avg
Total O_3 % change
Mean Age (yrs)
base, 1995 model
circulation cases
Kzz cases
gravity wave cases
Kyy cases
Kyy+circulation cases
combination cases
0.0
−0.1
−0.2
−0.3
−0.4
−0.5
−0.6
−0.7
−0.8
−0.9
−1.0
0
1
2
3
4
5
6
7
8
V
H
W
E
U
K
G
D
L
A
R
F
O
M
C
N
B
T
S

FIGURE 12

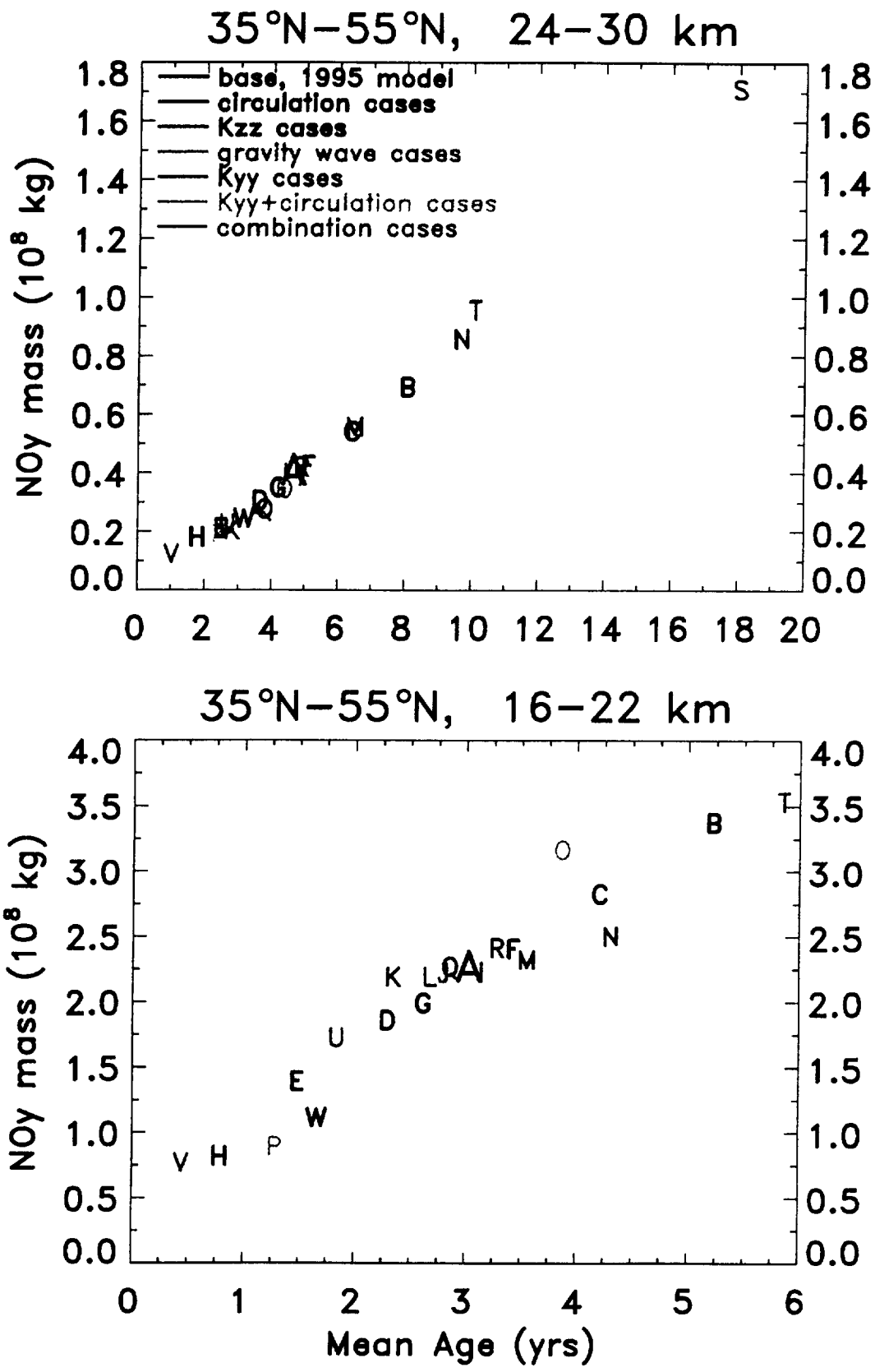
Age vs. NOy mass (A3), annual mean
35°N–55°N, 24–30 km
base, 1995 model
circulation cases
Kzz cases
gravity wave cases
Kyy cases
Kyy+circulation cases
combination cases
NOy mass (10^8 kg)
35°N–55°N, 16–22 km
Mean Age (yrs)

FIG. 13